acta physica slovaca vol. 52 No. 3, 123 – 141 **June 2002**

THE DC ELECTRICAL CONDUCTIVITY CALCULATION PURELY FROM THE DISSIPATIVE COMPONENT OF THE AC CONDUCTIVITY III. STATISTICAL ENSEMBLE INHERENT TO STATE WITH DC CURRENT

N. Milinski[1*], **E. Milinski** [†]

[*] *Institute of Fundamental Disciplines - FTN,*
University of Novi Sad, 21000 Novi Sad, Yugoslavia
[†] *SoftLaw Corporation, PO Box 772, Dickson ACT 2602, Australia*

Received 29 December 2001, in final form 10 April 2002, accepted 12 April 2002

Amorphous conductors such as liquid metals and alloys are subject to dc conductivity σ calculation here. Principal aim is to explore the impact on σ of the constitutive equation $\alpha^* = 1$, formulated and developed in the preceding papers. The nearly free electrons (NFE) model has been applied. Alkali metals are assumed to fit this model well, and sodium the best. Consequently, the results on these metals have been assumed reliable and relevant for conclusions making. The conclusion we made is: instead of the Fermi radius k_F proper for the statistical ensemble in state of thermodynamics equilibrium, a new k'_F number is needed to be introduced into the linear response formula when calculating σ and α^*. This k'_F is the length of the corresponding axis of ellipsoid proper for describing the statistical ensemble in the state with dc current. In the traditional interpretation of the linear response formula (Kubo formula) this conversion has been overlooked. Parameters of the mentioned ellipsoids are determined in this paper for a number of liquid metals of valency numbers 1,2,3,4, in addition to a selection of some binary and ternary conducting alloys. It is up to experimental measurements to decide how real this concept of restructuring the statistical ensemble is.

PACS: 02.50.+s, 05.60.+w, 72.15.-v

1 Introduction

This paper, following the two previous papers [1, 2] from this series, hereafter referred to as I., and II. respectively, is devoted to numerical calculation of σ, the dc electrical conductivity. Principal aim of this paper is to investigate the impact on σ of the explicit and consistent inclusion into calculation of the constitutive equation [2] $\alpha^* = 1$. This constitutive equation emerges from the equation: $\lim_{\omega\to 0} \sigma_i(\omega) = 0$, after the non-dissipative component $\sigma_i(\omega)$ of the full electrical conductivity $\sigma(\omega)$, frequency ω dependent, is substituted by the linear response expression for $\sigma_i(\omega)$, see eqs. (66), (67), (106) and (108) in II.

[1] E-mail address: ftn_mnik@uns.ns.ac.yu

The point of view we apply here is: σ and α^*, being them both related to the same state of a conductor, are to be calculated from the same set of input parameters, and the calculated α^* should obey the relation $\alpha^* = 1$ anyway. If the constitutive equation is not obeyed, the pattern of σ calculation cannot be assumed correct, irrespective to the results for σ, calculated for a given particular case. Since the nearly free electrons (NFE) model has been applied, well fitted to alkali metals, the results of calculations on these metals, are expected to be the most trusted and relevant items to discussion and conclusions making. It appeared that the relation $\alpha^* = 1$ has not been obeyed on alkali metals, including sodium, which is assumed to fit the (NFE) model the best, though the calculated σ agree well with the values obtained from experimental measurements. Having in mind this deficiency, on top of the objections, critical views and pleads for improvement [3–7] known from before, we have looked for outcome from this deficiency, and have found it in adopting some corrections concerning the concept of σ calculation. According to the Kubo's concept, dc conductivity has to be calculated by inserting into the linear response formula for σ the values of parameters characterizing the state of thermodynamics equilibrium. Now we assume, as far as Fermi radius k_F is concerned, this is not correct. In the state of thermodynamics equilibrium, the carriers of an amorphous conductor are represented by the statistical ensemble spherical in the wavenumbers space, in $k - space$, while in presence of the dc electric field, the carrier system has undergone conversion, and the corresponding statistical ensemble obtains an ellipsoidal shape in the wavenumber space, in $k - space$. The conversion is to be attributed to coupling to the dc electric field, uniform and long lasting on the microscopic scale. Some authors assume [4], this conversion is left out of the linear response theory as consequence of linearisation in external driving force applied in the too early stage of linear response formula derivation. Anyway, we assume now, instead of the Fermi radius k_F characteristic for thermodynamics equilibrium state, a new k'_F radius of the ellipsoid is to be substituted into the formula for σ and α^* calculation.

This paper is organized as follows. In Section 2.1 the matrix element U_q, being it the main component in expressions for σ and α^*, is outlined. Two types of U_q are shown. Section 2.2 is devoted to numerical calculation. The properties of two formulas, giving σ and α^* in terms of $S(q)$ — the structure factor, and $v(q)$ — the form-factor, are explained and monitored by a number of graphs. A table with results of calculation on alkali metals is given. The analysis of the results then follows, where the disobey of the equation $\alpha^* = 1$ has initiated a new treatment of the Fermi radius. In Section 2.3 the statistical ensemble for carriers, inherent to the state with dc current is introduced and described. Section 3 is devoted to calculation of σ and α^* on liquid metals from columns IIA, IIIA and IVA of the Periodic Table of the elements, in addition to some binary and ternary conducting alloys. Section 4 is devoted to conclusions.

2 Basics in σ calculation on amorphous conductors

2.1 The Matrix Elements $|U_q|$

We start with the coupling (scattering) Hamiltonian U, as it is given by the sum of overlapping potentials of single ions $u(r - R_j)$, multiplied by the carrier's charge $(-e)$

$$U(r) = -e \sum_j u(r - R_j), \tag{1}$$

where r and R_j are the carrier's and the ion's position, respectively. The matrix element U_q,

$$U_q =< \Psi_{k+q}|U|\Psi_k >, \tag{2}$$

with $U = U(r)$ given by eq. (1), and with Ψ_{k+q} and Ψ_k plane waves, reads

$$U_q = \left(\frac{-e}{V}\right) \int_V \sum_j u(r - R_j) \mathrm{e}^{-i\mathbf{q}\cdot\mathbf{r}} \mathrm{d}^3 r. \tag{3}$$

Following the Van Hove's path [9] of separating the structure-induced properties from the atom-induced properties in U_q, it is convenient to factories eq. (3) as

$$U_q = s_a(q) \cdot v(q), \tag{4}$$

where $s_a(q)$ and $v(q)$ are the structure-amplitude and the form-factor respectively, defined [8] by

$$s_a(q) = \frac{1}{N_a} \sum_j \mathrm{e}^{-i\mathbf{q}\cdot\mathbf{R_j}}, \tag{5}$$

$$v(q) = \left(\frac{-e}{\Omega}\right) \int_V \mathrm{d}^3 r \cdot u(r) \mathrm{e}^{-i\mathbf{q}\cdot\mathbf{r}}, \tag{6}$$

where N_a and Ω are the number of ions in the volume V and single ionic volume respectively, $\Omega = V/N_a$. In order to take into account screening, exchange and carrier's correlation effects [10, 11], $v(q)$ is rewritten as

$$v(q) = \frac{v^i(q)}{\epsilon_r(q)}, \tag{7}$$

where $\epsilon_r(q)$ is the relative dielectric screening function with the correlation and exchange effects included, and $v^i(q)$ is the bare-ion's form-factor. The bare-ion's form-factor $v^i(q)$ is obtained from eq. (6), after the single ion's screened potential $u(r)$ is replaced by the single ion's bare potential $u^i(r)$ [8, 10, 11]. Here we are going to outline explicitly two types of bare-ion's form-factors $v^i(q)$. The first one, in our terminology called the true-potential bare-ion form-factor $v^i(q)$, is obtained by taking for $u^i(q)$ the single ion's electrostatic potential at r, produced by the atomic nucleus consisting of Z protons positioned at the origin of space, at $r = 0$, in addition to the core electrons spread around the nucleus with the electron density $n_e(\rho)$

$$u^i(r) = \left(\frac{e}{4\pi\epsilon_0}\right) \left[\frac{Z}{r} - \int_V \mathrm{d}^3\rho \left(\frac{n_e(\rho)}{r - \rho}\right)\right]. \tag{8}$$

The core electron density $n_e(\rho)$, as well as the integral in eq. (6) with $u(r)$ replaced by $u^i(r)$, appear in physics of X-ray diffraction and in physics of electron diffraction on crystals [8]. The integral in eq. (6), for this case, has been solved in terms of a certain quantity f_q, leading to the following expression for $v^i(q)$

$$v^i(q) = \left(\frac{-e^2}{\epsilon_0\Omega}\right) \left(\frac{Z - f_q}{q^2}\right), \tag{9}$$

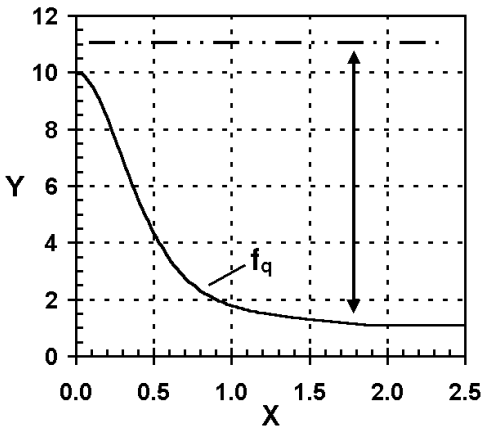

Fig. 1. Axes labeling: $X \equiv q[\,10^{10}\mathrm{m}^{-1}]$, $Y \equiv f_q$. q is the scattering's displacement wavenumber, f_q is the atomic scattering factor in electron units, here for sodium Na, with values taken from "The International Tables for X-ray Crystallography" [12]. The segment with arrows pointing to $q = 1.8 \cdot 10^{10}\mathrm{m}^{-1}$ by its own length displays magnitude of the term $Z - f_q$, standing as multiplier in eq. (9). For sodium $Z = 11$, and in the vicinity of the double Fermi wavenumber k_F, $q_0 = 2k_F \approx 1.8 \cdot 10^{10}\mathrm{m}^{-1}$, $f_q \approx 1$, therefore, in the vicinity of q_0, $Z - f_q \approx +10$.

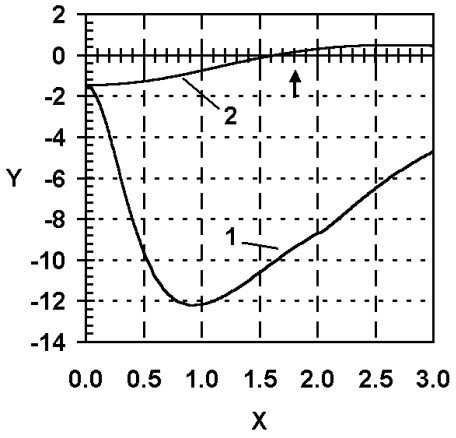

Fig. 2. Axes labeling: $X \equiv q[\,10^{10}\mathrm{m}^{-1}]$, $Y \equiv v(q)[\,1.6 \cdot 10^{-19}\mathrm{J}]$. Curves 1 and 2 are graphs of the true-potential form-factor and the pseudo-potential form-factor respectively, $v(q)$ given by eq. (7), with the same screening function $\epsilon_r(q)$ taking the correlation and exchange effects by the Kleinman-Langreth factor [11,16]. The bare-ion's form-factor $v^i(q)$ for curve 1 is given by eq. (9), for sodium Na with the parameters: $Z = 11$, $\Omega = 41.1 \cdot 10^{-30}\mathrm{m}^3$, and with f_q displayed in Fig. 1. The bare-ion's form-factor $v^i(q)$ for curve 2 is given by eq. (11), for Na with the parameters: $Z_v = 1$, $\Omega = 41.1 \cdot 10^{-30}\mathrm{m}^3$ and $R_c = 0.96 \cdot 10^{-10}\mathrm{m}$.

where ϵ_0 is the empty space dielectric constant (SI units are assumed). The term f_q is known under the name of the atomic scattering factor in electron units, and its numerical values, for any kind of neutral or ionized atom, are available from "The International Tables for X-ray Crystallography" [12]. The second type of bare-ion's form-factors, here denoted by $v^i_m(q)$, are known under the name of pseudo-potential or model-potential bare-ion's form-factors. Ashcroft's empty-core model-potential [10, 11], well representing this class of form-factors, is defined by

$$u^i_m(r) = \begin{cases} (eZ_v/4\pi\epsilon_0 r) & , r \geq R_c \\ 0 & , r < R_c \end{cases} \tag{10}$$

where Z_v and R_c are the atomic valency number and the empty-core radius respectively. The corresponding bare-ion form-factor $v^i_m(q)$, following from eq. (6) by substituting $u^i_m(r)$ for $u(r)$ in eq. (6), is

$$v^i_m(q) = \frac{-e^2 Z_v}{\epsilon_0 \Omega q^2} \cos(R_c q). \tag{11}$$

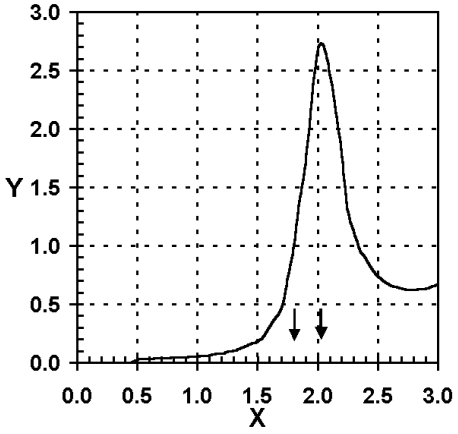

Fig. 3. Axes labeling: $X \equiv q[\,10^{10}\mathrm{m}^{-1}]$, $Y \equiv S(q)$. $S(q)$ is the structure factor for liquid sodium Na at temperature $t = 105^{\circ}$C, measured by X-ray diffraction [13]. Arrow pointing to $X = 1.8$ shows position of the double Fermi radius q_0, $q_0 = 2k_F = 1.8 \cdot 10^{10}\mathrm{m}^{-1}$. Arrow pointing to $X = 2.02$ shows position of q_p, the wavenumber corresponding to the first peak of the structure factor.

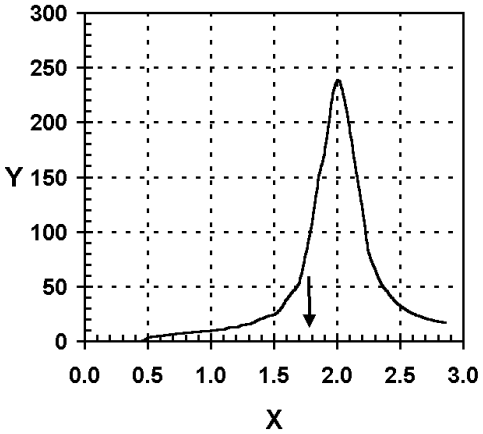

Fig. 4. Axes labeling: $X \equiv q[\,10^{10}\mathrm{m}^{-1}]$, $Y \equiv S(q)v^2(q)[\,1.6^2 \cdot 10^{-38}\mathrm{J}^2]$. The multipliers $v(q)$ and $S(q)$ defining Y in this graph are displayed by curve 1 in Fig. 2. and by the curve in Fig. 3. respectively. This graph displays the averaged square of the true scattering potential $|U_q|^2_{av}$ given by eq. (12), (up to the constant multiplier (Ω/V)), for the liquid sodium Na at temperature $t = 105^{\circ}$C. Arrow at $X = 1.8$ points to the double Fermi radius $q_0 = 2k_F = 1.8 \cdot 10^{10}\mathrm{m}^{-1}$.

The two types of form-factors from the above are different in their magnitude; the second type, given by eq. (11), is considerably smaller than the first one given by eq. (9). The reason why $v^i_m(q)$ is smaller than $v^i(q)$ given by eq. (9) is easy to understand, from comparison of eqs. (8) and (10). When right hand side of eq. (10) is inserted into eq. (6), the integral does not gain a contribution from the core sphere of radius R_c. Since R_c, by the concept's propositions is taken to be approximately equal to the positively charged ion's radius [10, 11], $v^i_m(q)$ describes a situation physically equivalent to one occurring when conduction electrons do not enter the core sphere at all. Unlike this, the form-factor eq. (9) describes the physical situation when carriers are allowed to enter the core sphere, with probability equal to any point of the V volume; note that the wave-functions Ψ_k in the matrix element eq. (2) are plane waves.

The structure induced properties of U_q, given by eq. (5), are determined by the set of $\mathbf{R}_j$ vectors, by the arrangement of ions. If the ions are arranged in a perfect crystalline lattice, $s_a(q) \neq 0$ only for $q = \kappa$, where κ denotes the reciprocal lattice vector, otherwise $s_a(q) = 0$. (In the cases of lattices with a single ion per unit cell, $s_a(\kappa) = 1$.) But if the ions are arranged outside the perfect crystalline structure, randomly, $s_a(q) \neq 0$ generally, for any wavenumber q.

To our purpose not U_q, but the square of it, averaged over time and configuration of ions, is needed, $|U_q|^2 = (U_q \cdot U_q^*)_{av}$, where the subscript $)_{av}$ means taking statistical average over the configuration and time. We transcribe $|U_q|^2$ to the form,

$$|U_q|^2 = \left(\frac{\Omega}{V}\right) S(q)v^2(q), \tag{12}$$

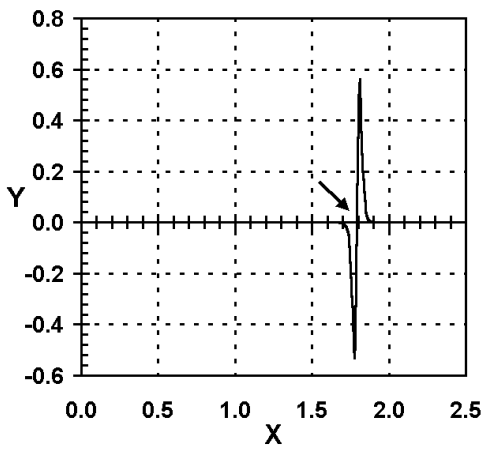

Fig. 5. Axes labeling: $X \equiv q[10^{10}\mathrm{m}^{-1}]$, $Y \equiv q^3 B_2(q)[10^{30}\mathrm{m}^{-3}]$. $B_2(q)$ as defined in eq. (15) depends on two parameters: temperature T, and Fermi energy E_f. This graph is for sodium Na at $t = 105^{\circ}$C, with $E_f = \hbar^2 k_F^2/2m_1$, for k_F and m_1 given in Tab. 1. Arrow at $X = 1.8$ points to the double Fermi radius, $q_0 = 2k_F = 1.8 \cdot 10^{10}\mathrm{m}^{-1}$.

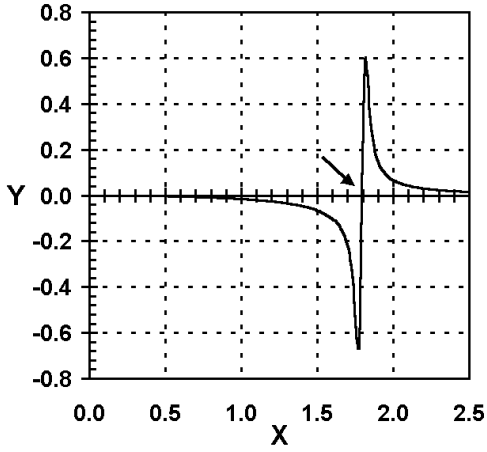

Fig. 6. Axes labeling: $X \equiv q[10^{10}\mathrm{m}^{-1}]$, $Y \equiv q^3 B_1(q)[10^{30}\mathrm{m}^{-3}]$. $B_1(q)$ defined by eq. (18) depends on two parameters: temperature T, and Fermi energy E_f. This graph is for sodium Na at $t = 105^{\circ}$C, with $E_f = \hbar^2 k_F^2/2m_1$, and with parameters k_F and m_1 given in Tab. 1. Arrow at $X = 1.8$ points to the double Fermi radius $q_0 = 2k_F = 1.8 \cdot 10^{10}\mathrm{m}^{-1}$.

where $S(q)$ is the structure factor defined by the expression

$$S(q) = \left(\frac{V}{\Omega}\right) |s_a(q)|^2_{av}. \tag{13}$$

Data for structure factors $S(q)$ of amorphous conductors, are available whether from experimental measurements [13, 14], or from analytical expressions derived for models, like the Percus-Yevick formula [8] is. In the numerical calculations within present paper, only the experimentally measured $S(q)$ are used, assuming that they are more reliable.

2.2 Numerical Calculations

The eq. (105) as it stands in our paper II., with $|U_q|^2$ substituted by eq. (12) from this paper, leads to the following expression for the dc conductivity σ,

$$\sigma = \left(\frac{\Omega e^2 \beta^2}{48 \cdot 6\pi^3 \hbar}\right) \left(\frac{m_1}{m_e}\right)^2 \int_0^{q_G} \mathrm{d}q \cdot q^3 \cdot S(q) \cdot v^2(q) \cdot B_2(q), \tag{14}$$

where the second derivative $\left(\partial^2 n_k/\partial \varepsilon_k^2\right)_{k=q/2}$, of the partition function n_k as accounted for $k = q/2$, has been replaced by a dimension-less function $B_2(q)$ in accord with the equations as follow

$$\left(\frac{\partial^2 n_k}{\partial \varepsilon_k^2}\right)_{k=q/2} = \beta^2 \cdot B_2(q), \qquad B_2(q) = n_{q/2} \cdot (1 - n_{q/2}) \cdot (1 - 2n_{q/2}), \tag{15}$$

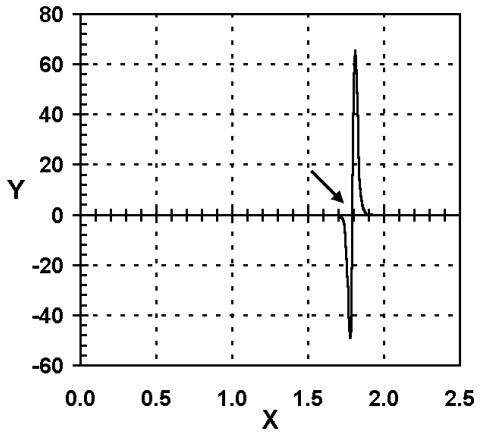

Fig. 7. Axes labeling: $X \equiv q[\,10^{10}\mathrm{m}^{-1}]$, $Y \equiv q^3 B_2(q) S(q) v^2(q)[\,1.6^2 \cdot 10^{-8}\mathrm{J}^2\mathrm{m}^{-3}]$. Y in this graph displays the integrand in eq. (14). The two factors of Y in this graph, i.e. $S(q)v^2(q)$ and $q^3 B_2(q)$ are displayed graphically in Fig. 4. and Fig. 5. respectively. Arrow at $X = 1.8$ points to the double Fermi radius $q_0 = 2k_F = 1.8 \cdot 10^{10}\mathrm{m}^{-1}$, (for sodium Na, at $t = 105^{\circ}$C).

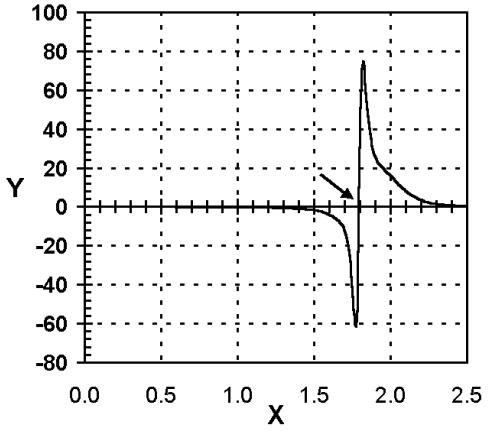

Fig. 8. Axes labeling: $X \equiv q[\,10^{10}\mathrm{m}^{-1}]$, $Y \equiv q^3 B_1(q) S(q) v^2(q)[\,1.6^2 \cdot 10^{-8}\mathrm{J}^2\mathrm{m}^{-3}]$. Y in this graph displays the integrand in eq. (17). The two factors of Y in this graph, i.e. $S(q)v^2(q)$ and $q^3 B_1(q)$ are displayed graphically in Fig. 4. and Fig. 6. respectively. Arrow at $X = 1.8$ points to the double Fermi radius $q_0 = 2k_F = 1.8 \cdot 10^{10}\mathrm{m}^{-1}$, (for sodium Na, at $t = 105^{\circ}$C).

$$n_{q/2} = \frac{1}{\mathrm{e}^{\beta(E/4 - E_f)} + 1}, \qquad E = \beta \frac{\hbar^2 q^2}{2m_1}, \qquad \beta = (1/k_B T), \tag{16}$$

where k_B, T and E_f are the Boltzmann constant, temperature and Fermi energy respectively.

By the same substitution performed to eq. (106) from the paper II., the following equation for the $\alpha^* - term$ follows:

$$\alpha^* = \frac{\Omega^2 m_e \beta}{12\pi^4 \hbar^2 Z_v} \left(\frac{m_1}{m_e}\right)^2 \int_0^{q_G} \mathrm{d}q \cdot q^3 \cdot S(q) \cdot v^2(q) \cdot B_1(q), \tag{17}$$

where the dimensionless multiplier $B_1(q)$ in the integrand is given by

$$B_1(q) = \mathcal{V}.\mathcal{P}.\left(\frac{1}{E}\right) \int_0^{\infty} \mathrm{d}Z \left(\frac{1}{\mathrm{e}^{Z - \beta E_f} + 1}\right) \left[\frac{1}{(\sqrt{E} - 2\sqrt{Z})^2} - \frac{1}{(\sqrt{E} + 2\sqrt{Z})^2})\right], \tag{18}$$

with Z representing the dimensionless energy of carriers, $Z = (\beta\hbar^2 k^2/2m_1)$. Z_v in eq. (17) is the valency number, the number of conduction electrons per ion, $(V/N) = (V/N_a \cdot Z_v) = \Omega/Z_v$. The integral in eq. (18) has no solution in terms of the elementary functions, and it has to be carried out numerically. Due to the singularity in the point $Z = (E/4)$, the numerical calculations are to be performed with much of care. The two functions from the above, $B_1(q)$ and $B_2(q)$, already have appeared in our earlier work [15], but in a different context, with tabulated values of function $B_1(q)$, for a series of βE_f parameters. The integrands in eqs. (14) and (17), can be expressed in terms of three functions of q as follow: $S(q)v^2(q)$, $q^3 B_2(q)$ and $q^3 B_1(q)$. The graphs of these functions displayed on characteristic samples, help us a lot, better to understand eqs. (14) and (17) as calculating tools, and to see the specific way in which the scattering Hamiltonian $|U_q|^2 \sim S(q)v^2(q)$ impacts σ and α^*.

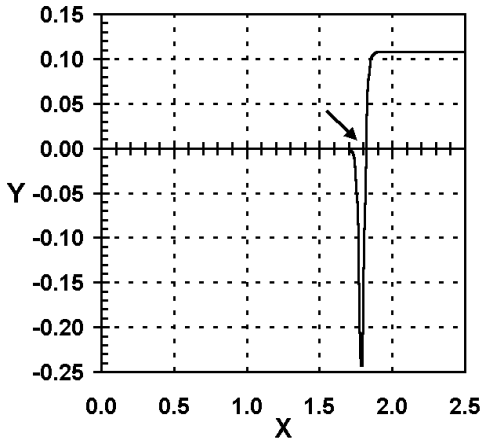

Fig. 9. Axes labeling: $X \equiv q_G[\,10^{10}\mathrm{m}^{-1}]$, $Y \equiv \sigma(q_G)[\,10^{8}(\Omega\cdot\mathrm{m})^{-1}]$. q_G denotes the upper limit of integration in eq. (14). $\sigma(q_G)$ in this graph is the conductivity σ as function of q_G, for sodium Na at $t = 105^{\circ}$C, with parameters given in Tab. 1. Arrow at $X = 1.8$ points to the double Fermi radius $q_0 = 2k_F = 1.8\cdot 10^{10}\mathrm{m}^{-1}$].

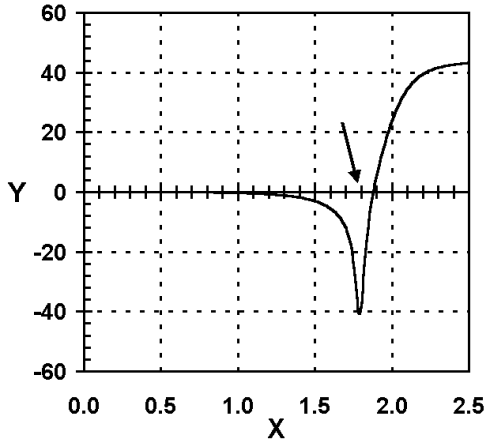

Fig. 10. Axes labeling: $X \equiv q_G[\,10^{10}\mathrm{m}^{-1}]$, $Y \equiv \alpha^*(q_G)$. q_G denotes the upper limit of integration in eq. (17). $\alpha^*(q_G)$ in this graph is the value of α^*-term as function of q_G, for sodium Na at $t = 105^{\circ}$C, with parameters given in Tab. 1. Arrow at $X = 1.8$ points to the double Fermi radius $q_0 = 2k_F = 1.8\cdot 10^{10}\mathrm{m}^{-1}$].

In Fig. 1, where f_q, the atomic scattering factor in electron units is displayed, the segment with arrow on both ends, represents the factor $(Z - f_q)$ appearing in eq. (9). Physically, $(Z - f_q)$ can be interpreted as the magnitude of the electric charge seen by the carrier scattered with a given displacement wavenumber q. In case of a displacement vector $q_0 = 2k_F = 1.8\cdot 10^{10}\mathrm{m}^{-1}$, the factor $(Z - f_q)$ has value, $(Z - f_q) \approx +10$, and it can be interpreted like if the carriers moving on the Fermi surface with wavenumber k_F, in the event of back scattering have seen the scatterer (Na-ion), with a charge of $+10$ units of electron charge, and it can be so only if the carriers have penetrated the Na-ion deep down, almost to the very bottom of the electronic core, leaving only one core electron closer to the atomic nucleus. How real this description may be, it is a matter to dispute, but eq. (9) gives it.

Figure 2 displays the graphs of the form-factors $v(q)$ given by eq. (7), with the screening function $\epsilon_r(q)$ accounting the correlation and exchange effects by means of the Kleinman Langreth factor [16], in this instance in application to sodium Na. Curve labeled by 1 is the true-potential form-factor given by eq. (9) and accounted for by the parameters for Na: $Z = 11$, $\Omega = 41.1\cdot 10^{-30}\mathrm{m}^3$, and f_q taken from "The International Tables for X-ray Crystallography" for sodium. Curve labeled by 2 is the Ashcroft's empty-core model-potential (pseudo-potential) given by eq. (11) with the parameters for Na: $Z_v = 1$, $\Omega = 41.1\cdot 10^{-30}\mathrm{m}^3$, $R_c = 0.96\cdot 10^{-10}\mathrm{m}$. It is the curve of type 1 which is applied in calculating σ within this work. Figure 3 displays the structure factor $S(q)$ for the case of liquid sodium Na at temperature $t = 105^{\circ}$C, with values obtained from X-ray measurements [13, 14]. Fig. 4 shows the graph of $S(q)v^2(q)$, as it is calculated from $v(q)$ presented by curve 1 in Fig. 2, and from $S(q)$ displayed in Fig. 3. Up to a constant multiplier (Ω/V), this curve displays the average of the true scattering potential $|U_q|^2_{av}$.

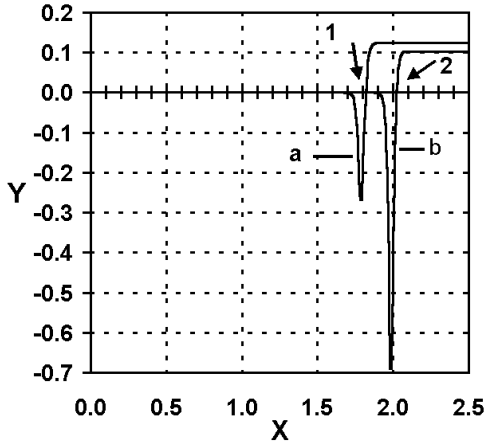

Fig. 11. Axes labeling: $X \equiv q_G[10^{10}\mathrm{m}^{-1}]$, $Y \equiv \sigma(q_G)[10^8(\Omega\cdot\mathrm{m})^{-1}]$. q_G denotes the upper limit of integral in eq. (14). $\sigma(q_G)$ denotes the conductivity σ as function of q_G, with parameters given in Tab. 1 for sodium Na at $t = 105^{\circ}$C. Curve a is calculated by taking for Fermi radius numerical value given in line 4, i.e. $k_F = 0.90\cdot 10^{10}\mathrm{m}^{-1}$, while curve b is calculated by the second selection for Fermi radius given in line 8, i.e. $k_F' = 0.99\cdot 10^{10}\mathrm{m}^{-1}$. All other parameters are the same for both curves. Arrow 1 points to the double Fermi radius $q_0 = 2k_F = 1.8\cdot 10^{10}\mathrm{m}^{-1}$, while arrow 2 points to the second selection of the double Fermi radius, $q_0^{'} = 2k_F' = 1.98\cdot 10^{10}\mathrm{m}^{-1}$.

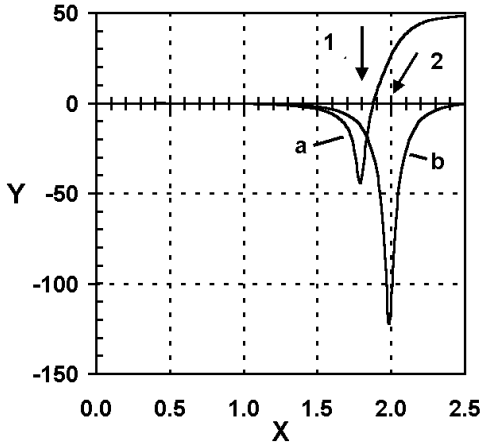

Fig. 12. Axes labeling: $X \equiv q_G[10^{10}\mathrm{m}^{-1}]$, $Y \equiv \alpha^*(q_G)$. q_G denotes the upper limit of integral in eq. (17). $\alpha^*(q_G)$ displays α^*-term as function of q_G, with parameters given in Tab. 1 for sodium Na at $t = 105^{\circ}$C. Curve a is calculated by taking for Fermi radius numerical value given in line 4, i.e. $k_F = 0.90\cdot 10^{10}\mathrm{m}^{-1}$, while curve b is calculated by the second selection for Fermi radius given in line 8, i.e. $k_F' = 0.99\cdot 10^{10}\mathrm{m}^{-1}$. All other parameters are the same for both curves. Arrow 1 points to the double Fermi radius $q_0 = 2k_F = 1.8\cdot 10^{10}\mathrm{m}^{-1}$, while arrow 2 points to the second selection of the double Fermi radius, $q_0^{'} = 2k_F' = 1.98\cdot 10^{10}\mathrm{m}^{-1}$.

The Fig. 5 and Fig. 6 display graphs of $q^3B_2(q)$ and $q^3B_1(q)$ respectively. These two functions act like moulds shaping the impact to σ and α^* of the scattering potential $|U_q|^2 \sim S(q)v^2(q)$. From the shape of the graph in Fig. 5 one can conclude that the multiplier $q^3B_2(q)$ in the integrand of eq. (14) cuts out a very narrow interval on the $q-axis$, with center at the point $q_0 = 2k_F$, where $q^3B_2(q) \neq 0$ and where the scattering potential $S(q)v^2(q)$ has impact to σ, and the remaining larger part of q-axis where $q^3B_2(q) \approx 0$, and where $S(q)v^2(q)$ has no impact to σ. The small width of the interval on q-axis giving non-zero contribution to σ, allows us to state that only the scattering back (or nearly back scattering) matters to σ calculated from eq. (14). From the shape of graph in Fig. 6, a similar conclusion can be formulated for the role played by the multiplier $q^3B_1(q)$ in the integrand of eq. (17). However, the width of q-interval, where $S(q)v^2(q)$ plays significant role in α^* calculation, is considerably larger than the width of the interval where $S(q)v^2(q)$ plays significant role in σ calculation. There is also another interesting feature common to both graphs in Fig. 5 and Fig. 6. It is the negative sign of both $q^3B_2(q)$ and $q^3B_1(q)$, for any $q < 2k_F$ and the positive sign of both $q^3B_2(q)$ and $q^3B_1(q)$, for any $q > 2k_F$, meaning that both σ and α^* gain negative contributions from the scattering with $q < 2k_F$, and correspondingly a positive one from the scattering with $q > 2k_F$, since the factor $S(q)v^2(q)$ is positive for any q. Therefore σ and α^* are equal to the differences of the mentioned positive and negative contributions.

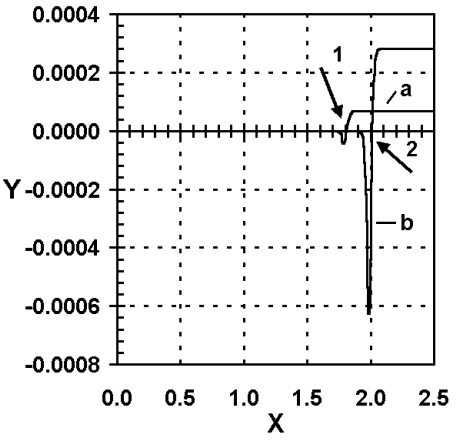

Fig. 13. Axes labeling: $X \equiv q_G[\,10^{10}\mathrm{m}^{-1}]$, $Y \equiv \sigma(q_G)[10^8(\Omega\cdot\mathrm{m})^{-1}]$. q_G is the upper limit of the integral in eq. (14). $\sigma(q_G)$ is the conductivity σ as function of q_G, with parameters given in Tab. 1 for Na at $t = 105^{\circ}$C. The parameters for curves a and b in both, this and Fig. 11 respectively are the same in everything but the form-factor $v(q)$. While in Fig. 11 the true-potential form-factor $v(q)$ has been applied, whose graph is given by curve 1 in Fig. 2, in this figure the pseudo-potential form-factor $v(q)$ has been applied, whose graph is given by curve 2 in Fig. 2 The arrow 1 points to the double Fermi radius $q_0 = 2k_F = 1.8\cdot 10^{10}\mathrm{m}^{-1}$, while the arrow 2 points to the second selection of the double Fermi radius, $q_0^{'} = 2k_F' = 1.98\cdot 10^{10}\mathrm{m}^{-1}$.

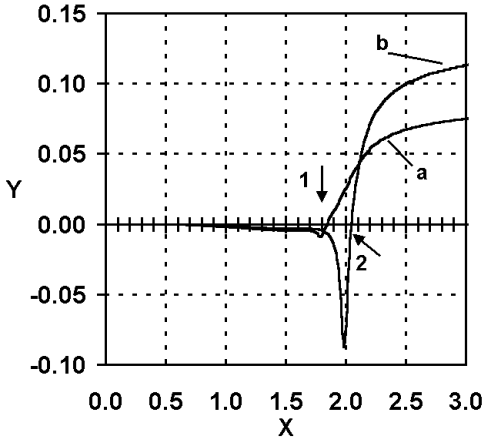

Fig. 14. Axes labeling: $X \equiv q_G[\,10^{10}\mathrm{m}^{-1}]$, $Y \equiv \alpha^*(q_G)$. q_G is the upper limit of the integral in eq. (17). $\alpha^*(q_G)$ is the $\alpha^* - term$ as function of q_G, with parameters given in Tab. 1 for Na at $t = 105^{\circ}$C. The parameters for curves a and b in both this and Fig. 12 respectively are the same in everything but the form-factor $v(q)$. While in Fig. 12 the true-potential form-factor $v(q)$ has been applied, whose graph is given by curve 1 in Fig. 2, in this figure the pseudo-potential form-factor $v(q)$ has been applied, whose graph is given by curve 2 in Fig. 2. Arrow 1 points to the double Fermi radius $q_0 = 2k_F = 1.8\cdot 10^{10}\mathrm{m}^{-1}$, while arrow 2 points to the second selection of the double Fermi radius, $q_0^{'} = 2k_F' = 1.98\cdot 10^{10}\mathrm{m}^{-1}$.

The graphs in Fig. 7 – Fig. 10, give further and quite convincing approval of back scattering character mattering to σ and α^*. From the graph in Fig. 9 we see that integration in eq. (14) up to the upper limit of integration $q_G = 1.7\cdot 10^{10}\mathrm{m}^{-1}$ does not result in any noticeable gain; the whole gain takes place on the interval of q from $1.7\cdot 10^{10}\mathrm{m}^{-1}$ till $1.9\cdot 10^{10}\mathrm{m}^{-1}$. The upper limit of integration in q denoted by q_G in eq. (14) was not specified so far, but now we see it may be extended till $q_G = \infty$, or it may be restricted to $q_G = 1.9\cdot 10^{10}\mathrm{m}^{-1}$ in this case, it gives the same σ. Generally, the upper limit of integration in eq. (14), q_G, is a number of order $q_0 = 2k_F$, slightly above this number. From observing the graph in Fig. 10 similar conclusions can be formulated about α^* and eq. (17), but with somewhat wider interval in the vicinity of point $q_0 = 2k_F$ being relevant to α^* calculation.

In Tab. 1, the result of our numerical calculations on five alkali metals at different temperatures are presented. The nearly free electrons (NFE) dynamics of carriers is applied in these calculations. Generally it is assumed that these metals meet the nearly free electrons (NFE) model well. Sodium Na is the one assumed to meet the (NFE) model the best. The results on sodium are assumed most reliable and relevant for conclusion and decision making.

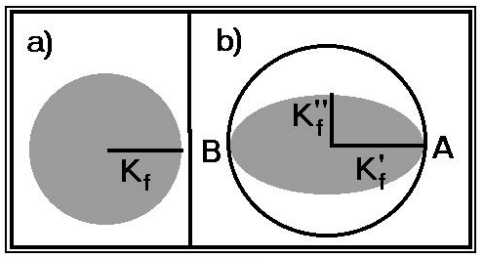

Fig. 15. In a) the shaded sphere with radius k_F represents the part of the $k-space$ occupied by conducting electrons in the state of thermodynamics equilibrium. In b) the shaded ellipsoid with the axis denoted by k'_F oriented toward the dc external electric field represents the part of the $k-space$ occupied by conduction electrons in the state of stationary but not thermodynamically equilibrium state. Volumes of both the sphere and the ellipsoid are equal, so is the number of carriers within them. Thermal smearing of states in the vicinity of the Fermi surface is not indicated in the figures, but it is assumed to exist and to be determined by the Fermi-Dirac distribution in both the sphere and the ellipsoid.

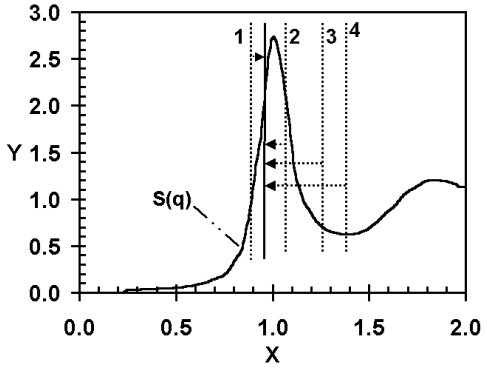

Fig. 16. Axes labeling: $X \equiv q$, $Y \equiv S(q)$. $S(q)$ is a schematic display of the structure factor, on $q-axis$ scaled by q_p, the position of the first pick of $S(q)$. The vertical dotted lines display the position of the double Fermi radius $2k_F$, relative to the first pick, for conductors of valency numbers: $Z_v = 1; 2; 3; 4$ respectively. In presence of the dc current, the carrier system undergoes a conversion in which $2k'_F$, double of the parameter k'_F defined in this paper, denoted by vertical straight full line, is positioned somewhere slightly below the position of the first pick of $S(q)$.

There are three facts to point out when estimating data in Tab. 1. First, all the parameters, as given in lines t, Ω, (m_1/m_e), k_F, and applied as inputs in calculating values of σ_{cal} and α^*_{cal}, are in pretty good consent with data encountered in sources of parameters for the liquid metals considered. Second, values of ρ_{cal} in Tab. 1, obtained from $\rho_{cal} = 1/\sigma_{cal}$ with σ_{cal} calculated by eq. (14), are in pretty good agreement with the experimental values of resistivity ρ_{exp} [21]. Third, the values of α^*_{cal} in Tab. 1 are in rather obvious disagreement with the theoretically prescribed value of α^*, $\alpha^* = 1$. Here we are facing a dilemma, whether to accept this situation as non-problematic, since ρ_{cal} is satisfactory, and to regard the mentioned disagreement as a marginal item, or alternatively to conceive this situation as a problematic one, assuming that the inconsistency between α^*_{cal} and $\alpha^* = 1$ is not marginal, but rather a symptom of a fault. We undertook the last option, anticipating that the source of fault is in wrong values for the input parameter denoted by k_F. After performing the calculations with taking for the input parameter k_F values as they are given in Tab. 1 by the row k'_F, we have obtained for resistivity ρ and the parameter α^* values as they are given in rows ρ'_{cal} and $(\alpha^*_{cal})'$. Resistivities ρ have been slightly changed but still remaining close to ρ_{exp}, while α^* has passed through significant conversion, (compare the row α^*_{cal} to row $(\alpha^*_{cal})'$), approaching the theoretically prescribed value of $\alpha^* = 1$.

Graphs in Fig. 11 and Fig. 12 give clear visualization of the conversion which σ_{cal} and α^*_{cal} pass through, when k_F has been shifted from $k_F = 0.896 \cdot 10^{10}\mathrm{m}^{-1}$ to $k'_F = 0.995 \cdot 10^{10}\mathrm{m}^{-1}$, in case of liquid sodium Na at temperature $t = 105^{\circ}$C. The transition from curve a to curve b in Fig. 11 and Fig. 12 proceeds gradually as the parameter k_F is rising from $k_F = 0.896 \cdot 10^{10}\mathrm{m}^{-1}$ to $k'_F = 0.995 \cdot 10^{10}\mathrm{m}^{-1}$. Similar are the graphs for all the remaining liquid metals in Tab. 1.

Liquid metal	Li	Li	Li	Na	Na	Na	Na	Na	K	K	K	K	K	Rb	Rb	Cs	Cs
$t\,[^{\circ}\mathrm{C}]$	190	250	452	105	200	300	450	550	70	105	200	350	450	40	200	30	200
$\Omega\,[10^{-30}\mathrm{m}^3]$	22.5	22.8	23.8	41.1	42.3	43.3	45.1	46.4	78.6	79.3	81.4	85.1	87.6	96.1	102	120.	127.
(m_1/m_e)	2.05	2.07	1.99	1.32	1.26	1.27	1.13	1.11	0.98	0.91	0.87	0.79	0.76	0.54	0.50	0.40	0.39
$k_F[10^{10}\mathrm{m}^{-1}]$	1.10	1.09	1.08	0.90	0.89	0.88	0.87	0.86	0.72	0.72	0.71	0.70	0.70	0.67	0.66	0.63	0.62
α^*_{cal}	10.0	9.67	8.74	44.2	38.2	34.	20.	14.	106.	73.	59.	32.	18.	58.	31.	50.	30.
$\rho_{cal}\,[10^{-8}\Omega\cdot\mathrm{m}]$	23.4	23.7	22.9	9.3	9.87	11.9	18.2	23.3	5.62	8.1	11.	22.5	33.9	21.	34.	51.	55.
$\rho_{exp}\,[10^{-8}\Omega\cdot\mathrm{m}]$	24.	26.	34.	9.7	13.4	18.	25.	30.	13.	15.3	21.6	31.6	38.2	23.	37.	37.	56.
$*$	$*$	$*$	$*$	$*$	$*$	$*$	$*$	$*$	$*$	$*$	$*$	$*$	$*$	$*$	$*$	$*$	$*$
$k'_F\,[10^{10}\mathrm{m}^{-1}]$	1.22	1.22	1.18	0.99	0.98	0.97	0.96	0.94	0.79	0.79	0.78	0.77	0.76	0.74	0.72	0.71	0.68
$k''_F\,[10^{10}\mathrm{m}^{-1}]$	1.04	1.03	1.03	0.86	0.85	0.84	0.83	0.82	0.69	0.69	0.68	0.67	0.67	0.64	0.63	0.59	0.59
$(\alpha^*_{cal})'$	0.94	1.01	1.01	1.1	0.7	1.2	0.9	0.9	0.97	1.1	1.1	1.1	0.95	2.9	-1.1	2.6	0.7
$\rho'_{cal}\,[10^{-8}\Omega\cdot\mathrm{m}]$	23.7	25.9	34.	9.8	13.4	18.2	25.	29.7	13.0	15.3	21.6	31.6	38.	22.8	36.	37.	56.
$(k'_F - k_F)/k_F$	0.12	0.12	0.10	0.11	0.11	0.10	0.10	0.10	0.10	0.10	0.10	0.10	0.09	0.09	0.09	0.12	0.10
$q_p[10^{10}\mathrm{m}^{-1}]$	2.50	2.50	2.44	2.02	2.02	2.02	2.02	2.02	1.62	1.62	1.62	1.62	1.62	1.52	1.52	1.45	1.44
$(q_p - 2k'_F)/q_p$	0.02	0.02	0.03	0.02	0.03	0.04	0.05	0.07	0.03	0.03	0.04	0.05	0.06	0.03	0.05	0.03	0.06
DOS	0.75	0.77	0.75	0.72	0.70	0.72	0.66	0.65	0.82	0.76	0.74	0.69	0.68	0.51	0.50	0.45	0.45
Z_v	1.	1.	1.	1.	1.	1.	1.	1.	1.	1.	1.	1.	1.	1.	1.	1.	1.

Tab. 1. The labels Li, Na, K, Rb and Cs in the top row denote Lithium, Sodium, Potassium, Rubidium and Cesium respectively. Any column comprises the set of input parameters and the corresponding values of σ and a^* calculated by eqs. (14) and (17) respectively, for metal denoted on the top of the column. The rows (entries) labeled by t and Ω, display the metals temperature and the single ions volume respectively. Ω is calculated from the relation $\Omega = (A/\rho)1.66$, where A is the atomic mass of a given metal in the atomic mass units (a.ra.w), and ρ is the metal's density at temperature t in [g·cm^{-3}] units. Data for density ρ are taken from [13]. The row labeled by (m_1/m_e) displays the velocity mass m_1 as ratio to the free electron mass m_e. The experimental data for this important input parameter are: for Li from thermal measurements [17] $(m_1/m_e) = 2.19$, and [18] $(m_1/m_e) = 2.4$; for Na from cyclotron resonance [19,20] $(m_1/m_e) = 1.24$, while the electronic specific heat has given [17] $(m_1/m_e) = 1.25$, and also [18] $(m_1/m_e) = 1.3$. Experimental data for potassium K are: from cyclotron resonance [19] $(m_1/m_e) = 1.21$, and from thermal measurements [17] $(m_1/m_e) = 1.23$. Data listed for (m_1/m_e) in this Table for Li and Na agree very well with the up mentioned experimantal data. The row k_F displays the Fermi radius proper for the statistical ensemble in state of thermodynamics equilibrium. k_F has been calculated from $k_F = (3\pi Z_v/\Omega)^{1/3}$, with valency number $Z_v = 1$. Rows labeled by a^*_{cal} and ρ_{cal} (with ρ_{cal} obtained from $\rho_{cal} = 1/\sigma_{cal}$), display the numbers calculated by eqs. (17) and (14) respectively, from measured structure factors $S(q)$ [13,14], and from true form-factors $v(q)$ given by eqs. (7) and (9). The atomic scattering factors f_g in eq. (9) have been taken from "The International Tables for X-ray Crystallography" [12], and the screening function $\epsilon_r(q)$ in eq. (7), has been calculated from the expression taking the correlation and exchange effects into account by the Kleinman-Langreth factor [11,16]. Data for Fermi radius in these calculations have been taken from the above mentioned row labeled by k_F. Row labeled by ρ_{exp} displays the measured resistivities [21]. The data in this Table laid below the row with labels $*$ (stars), belong to calculations performed in accord with the concept developed in this paper, and the explanations are given in the main text of the paper.

Liquid Metal	Mg	Ca	Sr	Ba	Al	Ga	In	Tl	Si	Gc	Sn	Pb
t [°C]	680.	850.	780.	730.	670.	50.	160.	315.	1460.	980.	250.	340.
Ω [10^{-30}m^3]	26.1	48.5	61.1	68.6	18.9	19.	27.1	30.1	18.	21.7	28.4	32.3
(m_1/m_e)	1.00	0.65	0.42	0.275	1.	0.75	0.482	0.34	0.81	0.60	0.395	0.295
k_F [10^{10}m^{-1}]	1.31	1.07	0.99	0.95	1.67	1.67	1.48	1.43	1.88	1.76	1.61	1.54
α^*_{cal}	$-17.$	$-27.$	-25	$-17.$	-8.9	$-39.$	$-20.$	$-13.$	-3.85	-9.2	-7.5	-7.4
ρ_{cal} [$10^{-8}\Omega\cdot$m]	$-47.$	$-56.$	$-117.$	$-253.$	$-271.$	$-6766.$	$-882.$	$-836.$	$-427.$	$-313.$	$-1715.$	$-2600.$
ρ_{exp} [$10^{-8}\Omega\cdot$m]	27.6	33.	(58)	(133.)	24.2	26.2	33.	73.5	78.	70.	47.5	95.
*	*	*	*	*	*	*	*	*	*	*	*	*
k'_F [10^{10}m^{-1}]	1.153	0.88	0.848	0.830	1.275	1.20	1.112	1.062	1.10	1.00	1.059	1.054
k'' [10^{10}m^{-1}]	1.39	1.18	1.07	1.02	1.91	1.97	1.71	1.66	2.46	2.33	1.98	1.86
$(\alpha^*_{cal})'$	0.97	1.02	1.	1.	1.	1.	1.	1.	1.	1.	1.	1
ρ'_{cal} [$10^{-8}\Omega\cdot$m]	27.6	32.3	58.9	131.	24.2	28.	32.8	73.5	78.	70.	47.5	96.
$(k'_F - k_F)/k_F$	-0.12	-0.18	-0.14	-0.15	-0.24	-0.28	-0.25	-0.26	-0.41	-0.43	-0.34	-0.32
q_p [10^{10}m^{-1}]	2.44	1.97	1.80	1.75	2.71	2.52	2.30	2.28	2.72	2.55	2.22	2.28
$(q_p - 2k'_F)/q_p$	0.055	0.107	0.058	0.05	0.059	0.048	0.033	0.068	0.18	0.21	0.046	0.075
DOS [st./eV·atom]	0.40	0.37	0.29	0.21	0.32	0.23.	0.195	0.146	0.218	0.17	0.16	0.135
Z_v	2.	2.	2.	2.	3.	3.	3.	3.	4.	4.	4.	4.

Tab. 2. Parameters used in σ and α* calculation by eqs. (14) and (17) respectively, and results obtained on liquid metals from columns: IIA, IIIA, IVA of the Periodic Table of the elements, for temperatures *t* slightly above the melting point. Entries (left column of Table) and the labelings are the same as in Tab. 1. Ω is calculated from $\Omega = (A/\rho)1.66$, with A as the atomic mass of a given metal in the atomic mass units [a.m.u], and ρ is the metal's density at temperature t in $[\mathrm{g}\cdot\mathrm{cm}^{-3}]$ units. Data for metals density ρ are taken from [13]. Data for k_F have been calculated from $k_F = (3\pi^2 Z_v/\Omega)^{1/3}$ with valency number Z_v given in this Table. Data for measured resistivity ρ_{exp} are taken from [21]. α^*_{calc}, and resistivity ρ_{cal}, with ρ_{cal} obtained from $\rho_{cal} = 1/\sigma_{cal}$, have been calculated by eqs. (17) and (14) respectively, from Fermi radius k_F proper for state of thermodynamics equilibrium, with $S(q)$ measured by X-ray diffraction [13]. We see, both of these, α^*_{cal}, and ρ_{cal}, with values presented in rows 6 and 7 are physically meaningless. The results of calculation obtained by applying the concept formulated in this paper are presented below the row labeled by * (stars), with explanations given in the main text. Essentially, the system of two equations: eqs. (14) and (17), has been applied within this concept to determine the two unknown parameters: (m_1/m_e) and k'_F respectively, in addition to *DOS* determined from eq. (21).

$Ca_{10}Mg_{90-x}Ga_x$	$x=0$	$x=0$	$x=10$	$x=10$	$x=15$	$x=15$	$x=20$	$x=20$	$x=30$	$x=30$	$x=40$	$x=40$
$S(q)$-type	X-ray	neut.	X-ray	neut.	X-ray	neut.	X-ray	neut.	X-ray	neut.	X-ray	neut.
T [K]	300	300	300	300	300	300	300	300	300	300	300	300
Ω [10^{-30}m^3]	25.1	25.1	24.1	24.1	23.2	23.2	22.6	22.6	21.7	21.7	21.0	21
(m_1/m_e)	0.70	0.64	0.595	0.53	0.52	0.49	0.47	0.62	0.46	0.45	0.42	0.415
k_F [10^{10}m^{-1}]	1.33	1.33	1.37	1.37	1.40	1.40	1.42	1.42	1.46	1.46	1.50	1.50
α^*_{cal}	$-21.$	$-21.$	$-28.$	-28	$-8.$	$-8.$	-6.6	-6.6	-4.1	-3.78	-3.1	-3.2
ρ_{cal} [$10^{-8}\Omega\cdot$m]	$-143.$	$-143.$	$-486.$	-486	$-1049.$	-1049	$-1040.$	-1040	$-496.$	$-1752.$	$-760.$	$-890.$
ρ_{exp} [$10^{-8}\Omega\cdot$m]	53.	53.	101.	101.	130.	130.	159.	159.	214.	214.	193.	193.
*	*	*	*	*	*	*	*	*	*	*	*	*
k'_F [10^{10}m^{-1}]	1.172	1.175	1.18	1.16	1.165	1.14	1.146	1.142	1.13	1.10	1.14	1.12
k''_F [10^{10}m^{-1}]	1.42	1.42	1.48	1.49	1.53	1.55	1.58	1.58	1.66?	1.68	1.72	1.74
$(\alpha^*_{cal})'$	1.10	0.98	0.96	0.97	1.02	1.02	1.00	1.01	0.49	0.79	0.57	1.07
ρ'_{cal} [$10^{-8}\Omega\cdot$m]	53.	53.	101.	102.	128.	130.	156.	158.	208.	210.	217.	194.
$(k'_F-k_F)/k_F$	-0.12	-0.12	-0.14	-0.15	-0.17	-0.18	-0.19	-0.20	-0.18	-0.18	-0.24	-0.25
q_p [10^{10}m^{-1}]	2.43	2.42	2.48	2.44	2.51	2.44	2.50	2.46	2.52	2.52	2.52	2.52
$(q_p-2k'_F)/q_p$	0.037	0.029	0.048	0.047	0.072	0.066	0.083	0.08	0.010	0.13	0.091	0.11
DOS [st./eV·atom]	0.28	0.25	0.23	0.20	0.19	0.17	0.16	0.21	0.27	0.14	0.13	0.13
Z_v	2.0	2.0	2.1	2.1	2.15	2.15	2.2	2.2	2.3	2.3	2.4	2.4

Tab. 3. Input parameters and results in σ and a^* calculation by eqs. (14) and (17) respectively, on conducting alloys $Ca_{10}Mg_{90-x}Ga_x$ (x = 0; 10; 15; 20; 30; 40). Entries (left column of Table) and the labelings are the same here as in Tab. 1. For any x there are two columns of data: the left column, in the entry $S(q)$-type holding the sign X-ray, where the structure factor $S(q)$ applied has been obtained from X-ray diffraction technique, and the right column denoted by neut., where the structure factor $S(q)$ applied has been obtained by neutron diffraction technique [23–25]. f_q, the atomic scattering factors in electron units, needed in eq. (9), have been calculated by the formula: $f_q = C_1\cdot(f_q)_1 + C_2\cdot(f_q)_2 + C_3\cdot(f_q)_3$, where C_1, C_2 anf C_3 are the concentration of atoms Ca, Mg, and Ga respectively in the given alloy, and $(f_g)_1$, $(f_g)_2$ and $(f_g)_3$ are the atomic scattering factors in electron units taken from [12] for Ca, Mg and Ga respectively. Ω and k_F have been calculated from the valency number Z_v and mass density taken from [23–25]. Data for measured resistivity ρ_{exp} are taken from [23–25]. Resistivity $\rho_{cal} = 1/\sigma_{cal}$, and α^*_{cal} calculated by eqs. (14) and (17) respectively, from Fermi radius k_F proper for the state of thermodynamics equilibrium are both physically meaningless. The results of calculation obtained by applying the concept established in this paper are given in lines below the labels * (stars). Essentially, the system of two equations: eqs. (14) and (17), has been applied here to determine the two unknown parameters: (m_1/m_e) and k'_F respectively, in addition to *DOS* determined from eq. (21). More explanation is given in the main text.

Relative shift in k_F described by $(k'_F - k_F)/k_F$, as it is given in Tab. 1, needed to set $\alpha^*_{cal} \approx 1$, is nearly the same for all five liquid metals observed, it is nearly 10%. Second item observed in Tab. 1 is the property of the double of k'_F to remain below the q_p, with q_p denoting the position of the first pick of the structure factor $S(q)$,

$$2k'_F < q_p. \tag{19}$$

We assume, these particular cases give us a clue how to proceed in other cases of this kind (not necessarily metals in liquid phase), to set α^*_{cal} consistent with the theoretically prescribed value $\alpha^* = 1$, to obtain $\alpha^*_{cal} \approx 1$, and to determine $\rho_{cal} = 1/\sigma_{cal}$ afterwards, consistent with $\alpha^*_{cal} \approx 1$.

It is to be stressed that true-potential form-factors $v(q)$, given by eqs. (7) and (9) have been applied in the calculations presented in Tab. 1. The pseudo-potential form-factors are not applicable in this calculation. Fig. 13 and Fig. 14, display $\sigma_{cal}(q_G)$ and $\alpha^*_{cal}(q_G)$, the values of σ_{cal} and α^*_{cal} against q_G, with q_G denoting the upper limit of integration in q, for the case when $v(q)$ in eqs. (14) and (17) have been substituted by the pseudo-potential form-factor given by eqs. (7) and (11). We see that $\alpha^*_{cal}(q_G)$ is too small, and can't reach the theoretically prescribed value of $\alpha^* = 1$, independently on both the value of the upper integration limit q_G and of the chosen value for k_F. Similarly, the value of $\sigma_{cal}(q_G)$ is too small with this $v(q)$, and the calculated resistivity $\rho_{cal} = 1/\sigma_{cal}$ is too large, inconsistent with experimentally measured values of ρ_{exp}. This is true in all cases of liquid metals in Tab. 1. Obviously, the reason for non-applicability of the pseudo-potential form-factors in our approach to σ and α^* calculation is the smallness of the pseudo-potential form-factors.

2.3 Statistical ensemble for carriers inherent to state with dc current

The carriers system of a conductor, isotropic one like the liquid metals are, while the conductor itself is in the thermodynamics equilibrium, with no coupling to the external electric field, is described by the Fermi-Dirac statistical ensemble, presented by a sphere of radius k_F (Fermi radius) in the space of wavenumbers k, like it is illustrated in Fig. 15a). The fluctuation-dissipation theorem, and Kubo formula within its framework [22], is assumed to describe electrical conductivity σ from spontaneous thermodynamic fluctuations of the carrier's velocity taking place in the system, while the system itself is in the state of thermodynamics equilibrium, i.e. in the state described by the statistical ensemble presented in Fig. 15a). Our calculations, while performed in the framework of this concept, have lead to results presented in lines α^*_{cal} and ρ_{cal} in Tab. 1, which show internal inconsistency with the theory itself (conflict of α^*_{cal} with theoretically prescribed $\alpha^* = 1$). By taking instead of the Fermi radius k_F proper for the state of thermodynamics equilibrium, a larger one k'_F presented in the Tab. 1 below the line with labels $*$, the calculated numbers for α^* and resistivity ρ as presented in lines $(\alpha^*_{cal})'$ and ρ'_{cal}, became consistent with both theoretically prescribed $\alpha^* = 1$ and measured resistivity ρ_{exp}. What does this k'_F represent itself? Fermi radius k_F is not a dummy number allowing volatile physical interpretation, but it has very clear and tangible meaning; it determines the number of carriers in the system. When we have substituted for k_F in eqs. (14) and (17) the numbers k'_F, we did not have in mind the idea that the number of carriers is changed, but the idea that the statistical ensemble has changed its shape in the $k - space$. The ensemble is no longer spherical but rather it is of an ellipsoidal

shape, elongated in the direction of the external electric field, and thinned in the directions orthogonal to the electric field, with the remaining two axis of the ellipsoid equal to k''_F, keeping the volume of the ellipsoid equal to the volume of the Fermi sphere with radius k_F, therefore with the number of carriers unchanged, see Fig. 15b). The parameter k''_F in Tab. 1, has been calculated from the equation,

$$\frac{4}{3}\pi k_F^3 = \frac{4}{3}\pi k'_F \cdot (k''_F)^2. \tag{20}$$

Of course, a question can be raised now, how can we apply eqs. (14) and (17) to the system whose statistical ensemble is of ellipsoidal shape in $k - space$, if eqs. (14) and (17) themselves have been derived for spherical shape. It is the property of eq. (14) to give nonzero contribution only from back scattering, which enables it. Nonzero contribution to σ comes only from processes starting from points on one longest apex, denoted by A in Fig. 15b) and ended at the other opposite apex, denoted by B. The distance between the points A and B is $2k'_F$, i.e. the points A and B are in the same time on the sphere of radius k'_F and on the ellipsoid whose longest axes is k'_F. The same arguments hold up for eq. (17), but less accurately, since the back scattering property is less accurately pronounced in eq. (17).

The next question is: What kind of statistical ensembles is that one of ellipsoidal shape in Fig. 15b), is it a thermodynamics equilibrium state? We assume it is not, it is a non-equilibrium state, but stationary in time, holding up as long as dc electric field is present. Its energy (free energy) is over the carrier system's energy in the state of thermodynamics equilibrium, and as soon as the dc electric field is switched off, the process of system's return into the thermodynamics equilibrium starts. Theoretical description of the system's return into statistical equilibrium is hardly tractable in the framework of the Liouville equation, since it does not proceed with system's entropy invariant. The same is true for the reverse transition of the system from thermodynamics equilibrium into the stationary non-equilibrium state at the start of dc current. However it does not preclude the linear response formula for $\sigma(\omega)$ (Kubo formula) to be valid. When deriving it [22], one has to assume that the system's transition from the thermodynamics equilibrium into the mentioned stationary state already has been accomplished, and after that the system proceeds with system's entropy invariant, since the entropy produced in the carriers system equals the entropy flown out from the carriers system. Application of the Liouville equation to the posterior evolution is lawful, and the statistical operator of the initial state denoted by ρ_0, which the formula for $\sigma(\omega)$ is resting on [22], has to be assumed identical to the mentioned ellipsoidal stationary state. The important property here, the absence of macroscopic current in the initial state, has been kept.

We know, statistical ensemble is not the many particle system itself, but only a notion, a simplified scheme, sophisticated enough to reproduce the pattern of the many-particle system on a given level of observation, under the given boundary conditions [7]. From our calculation follows the conclusion that the statistical ensemble adequate for description of the thermodynamics equilibrium is not sophisticated enough to describe the state with dc current.

The need to introduce a correction concerning the initial state has been a subject of argumentation in a number of papers [3–6].In the papers by Ichiyanagi [5], where the problem of initial state determination for Kubo formula, has been treated by means of the Liouville equation, we can see how complex and volatile in practice would be the theoretical determination of the initial state. Instead, here we have found an approximation for it, in the above described ellipsoidal

model, whose parameters, the ellipsoid's axis lengths, can be determined from one accurately established requirement, from the equation $\alpha^* = 1$. Direct experimental test for correctness of this model is difficult no more than the direct experimental detection of the Fermi surface.

As far as dc conductivity is in question, we assume, the linear response formula has to be conceived as an algorithm determining σ from spontaneous thermodynamic fluctuations, taking place in the system which itself is no longer in the thermodynamics equilibrium, but it is shifted from it into some other, specific stationary state, like it is illustrated in Fig. 15.

3 Further calculations on liquid metals and conducting alloys

Calculation of σ and α^* on some other liquid metals, by applying the concept established in the preceding sections, is presented in Tab. 2. On top of Tab. 2, sequentially one after the other follow at first four metals from column IIA of the Periodic Table of the elements, then four metals from column IIIA, and finally four metals from column IVA. Only a single temperature slightly above the melting point is embraced in this Table.

Some elements from the set of input parameters for σ and α^* calculation by eqs. (14) and (17), can be assumed well known, whether from theory or from measurements independent of σ. Such parameters are: T — temperature, Ω — the single ion's volume; k_F-Fermi radius; $S(q)$-structure factor, f_q — atomic scattering factor in electron units and $\epsilon_r(q)$ — the screening function. However, one of the input parameters playing important role, the carriers velocity masses (m_1/m_e), is far from being known reliably for all metals in Tab. 2. There is also one parameter more, introduced by our concept, k'_F, which is unknown. Therefore, we are before the calculation of two terms: σ and α^*, with two missing parameters: (m_1/m_e) and k'_F respectively. Since α^* is always due to have the same value, $\alpha^* = 1$, if σ is known (taken) from measurements, then the two independent eqs. (14) and (17) can be conceived as a system suitable for determination of the two unknown parameters: (m_1/m_e) and k'_F. Tab. 2 is to be understood exactly this way, as presenting the numerical values of (m_1/m_e) and k'_F obtained by fitting to measured conductivity $\sigma_{exp} = 1/\rho_{exp}$, with ρ_{exp} listed in Tab. 2.

In all metals in Tab. 2, double of Fermi radius k_F is larger than q_p, $2k_F > q_p$, with q_p denoting the position of the first pick (principal maximum) of the structure factor $S(q)$. It has appeared that for all k'_F obtained by the fitting procedure, the double of k'_F is slightly below the first pick, $2k'_F < q_p$, in accord with eq. (19) deduced earlier for metals of valency number $Z_v = 1$. Fig. 16 illustrates the relation holding up for k_F, k'_F and q_p generally. We see, for any metal with $Z_v \geq 2$ holds $k'_F < k_F$.

The eq. (82) from our paper II., gives $N(\varepsilon_f)$, the density of states at Fermi surface, in units of (SI) system: $N(\varepsilon_f)$ [number of electron states/$\mathrm{J}\cdot\mathrm{m}^3$]. Equivalent to $N(\varepsilon_f)$ is the term usually denoted by DOS, and defined by

$$DOS = N(\varepsilon_f)\cdot e\cdot\Omega = \frac{k_F\, m_1\, e\,\Omega}{\pi^2\hbar^2}, \tag{21}$$

giving the density of states in units outside the (SI) units system:
DOS [number of electron states/$(\mathrm{eV})\cdot\mathrm{atom}$]. Data for DOS as given in Tab. 1, Tab. 2, and Tab. 3, have been calculated by eq. (21), but with k_F replaced by k'_F, in accord with our concept.

The results of calculation on a series of solid amorphous alloys $Ca_{10}Mg_{90-x}Ga_x$, (x=0; 10; 15; 20; 30; 40), are given in Tab. 3. Specific to Tab. 3 is that for any alloy (any x) there are two sets of results obtained from different structure factors $S(q)$ [23–25].The left column is calculated by $S(q)$ obtained from X-ray diffraction technique, while the right column is calculated by $S(q)$ obtained from neutron diffraction technique. For any x, up to $x = 20$ the results in two columns are in pretty good agreement, but for $x = 30$ and $x = 40$ some confusing differences between them exist.

Further investigation of conducting alloys, binary and ternary before all, can be very useful for verification of the concept exposed. Lack of measured (tabulated) structure factors $S(q)$ in the referential literature seems to exist.

4 Conclusion

This paper, third in sequence of papers on this subject, is devoted to detailed demonstration of σ calculation, in conjunction with the constitutive equation, introduced and developed in the two preceding papers. The traditional interpretation of the linear response formula (Kubo formula), prescribes to calculate σ from parameters taken for the thermodynamics equilibrium state. It has appeared that sensible interpretation of results, obtained by means of our consequently linear response calculation, requires a new, improved way of input parameters selection. We have concluded that the carrier system while exposed to boundary conditions creating dc current, cannot be described in terms of a statistical ensemble adequate to thermodynamically equilibrium state, spherical in the wavenumber space, in $k - space$, but rather in a new specific state, stationary state, ellipsoidal in shape, in the $k - space$. Instead of the Fermi radius k_F, a new k'_F parameter, one of the ellipsoid's axis is to be applied in σ calculation. The difference between k_F and k'_F is large enough to be measurable. It is to be stressed, that the replacement of k_F by k'_F in our calculation is not just a formal step, but it expresses the physics, the real conversion, the carrier system is undergone while the dc current is running in it. A desirable test to verify reality of our concept would be the experimental detection of difference between k_F and k'_F.

Acknowledgement: The authors are grateful to Dr. Nobuhiko Takeichi, of Nagoya University Japan, for providing us with $S(q)$ measured on $Ca_{10}Mg_{90-x}Ga_x$. The Institute of Physics in Zemun-Belgrade, and the Institute of MTA-KFKI in Budapest, are acknowledged for facilitating our use of books and journals in their libraries. Thanks are due to "Acta Physica Slovaca" for many constructive suggestions in the course of publication of results of this scientific project.

References

[1] N. Milinski, E. Milinski: *Acta Phys. Slov.* **50** (2000) 235
[2] N. Milinski, E. Milinski: *Acta Phys. Slov.* **51** (2001) 211
[3] N. G. Van Kampen: *Phys. Norveg.* **5** (1971) 279
[4] M. Wagner: *Phys. Rev.* **B 45** (1992) 11595
[5] M. Ichiyaqnagi: *J. Phys. Soc. Jpn.* **58** (1989) 2297
[6] M. Hutter, H. C. Ottinger: *Phys. Rev.* **E 54** (1996) 2526
[7] M. Grmela, H. C. Ottinger: *Phys. Rev.* **E 56** (1997) 6620

[8] N. E. Cusack: *The Physics of Structurally Disordered Matter*, Adam Hilger, Bristol-Philadelphia 1988

[9] L. Van Hove: *Phys. Rev.* **95** (1954) 249

[10] V. Heine, M. L. Cohen, D.Weaire: *Solid State Phys. vol. 24. The Pseudopotential Concept*, Academic Press, New York-London 1970

[11] W. A. Harrison, *Pseudopotential in the Theory of Metals*, Benjamin, New York 1966

[12] *The International Tables for X-ray Crystallography*, Kynoch Press, Birmingham 1962

[13] Y. Waseda: *The Structure of Non-Crystalline Materials, Liquid and Amorphous Solids*, MacGraw-Hill, New York 1980

[14] W. Van der Lugt, B. P. Alblas in: *Handbook of Thermodynamic and Transport Properties of Alkali Metals*, ed. R. W. Ohse; Blackwell Scientific 1985

[15] N. Milinski: *J. Phys. Soc. Jpn.* **51** (1982) 3977

[16] P. L. Rositer: *The electrical resistivity of metals and alloys*, University Press, Cambridge 1987

[17] A. P. Cracknell, K. C. Wong: *The Fermi Surface*, Clarendon Press, Oxford 1973

[18] K. Mendelssohn: *Cryophysics*, New York 1960

[19] D. Shoenberg, in: *The Physics of Metals I. Electrons*, ed. J. M. Ziman; The University press, Cambridge 1973

[20] C. G. Gremes, A. F. Kip: *Phys. Rev.* **132** (1963) 1991

[21] C. I. Smithells: *Metals Reference Book*, Butterworth & Co., London & Boston 1976

[22] D. N. Zubarev: *N*onequilibrium Statistical Thermodynamics, Nauka, Moskow 1971

[23] U. Mizutani: in *Materials Science, Technology vol. 3 Chap. 9*, ed. R. W. Cahn, P. Haasen, E. J. Kramer; Weinheim 1993, pp. 97-157

[24] N. Takeichi, T. Fukunaga, U. Mizutani: *J. Phys.: Condens. Matter* **10** (1998) 10179

[25] N. Takeichi, H. Sato, T. Fukunaga, U. Mizutani: *J. Phys.: Condens. Matter* **10** (1998) 10193